JOURNAL OF MATERIALS SCIENCE 33 (1998) 4239–4248

Effect of friction between fiber and matrix on the fracture toughness of the composite interface

A. T. DIBENEDETTO, M. R. GURVICH
Institute of Materials Science, U-136, University of Connecticut, Storrs, CT 06269, USA
E-mail: adiBened@mail.ims.nconn.edu

A method of evaluating the interfacial fracture toughness using a single-fibre composite test is proposed. In contrast with the existing techniques, the method takes into account the phenomenon of friction between the fibre and matrix in the debonding zone. A general mathematical solution of the problem and modelling of the friction phenomenon are presented. Finite-element analysis using a ''contact'' statement is utilized for numerical evaluation of the stress–strain state. The influence of the coefficient of friction and interfacial debonding length is analysed in detail. It is shown that the friction reduces the calculated value of the elastic strain energy release rate for a given debonding length, relative to that obtained when friction is neglected. The magnitude of the difference depends on the coefficient of friction, the elastic properties of the fibre and matrix, and the characteristics of the debonding mechanism. Experimental data on debonding in a series of glass-epoxy single-fibre composites are analysed using the proposed numerical technique to obtain the effects of fibre surface treatments and fibre strain-to-break on the interfacial fracture toughness. © *Kluwer Academic Publishers*

1. Introduction

The properties of interfaces between fibres and matrix in fibre-reinforced composites have a profound effect on the strength and durability of the material [1]. From the mechanical viewpoint, the main function of the interface is the transfer of stress between fibre and matrix both before and during the process of failure. Because composite failure is usually a multi-step process of fibre breaks [2– 6], the strength of the interface will affect the development of critical-size defects in the material. A limited amount of debonding at the site of a single-fibre fracture, for example, can provide a mechanism for crack-tip blunting, which may increase the toughness of the material with a tolerable loss of composite ultimate strength. Thus, there is a significant interest in characterization, analysis, and improvement (optimization) of the interface behaviour.

Experimental measurement and analysis of the interfacial strength and toughness in single-fibre composites has been reviewed extensively in the literature (e.g. [1, 7–16]). Different approaches regarding the analysis of the rate of release of the mechanical energy during debonding of the matrix from the fibre have been considered [17–23]. One method proposed [16, 24, 25] uses a finite element analysis of the strain energy release rate, along with an experimental measurement of the interfacial debonding length. Calculated values of the elastic strain energy release rate, G_{int}, i.e. the interfacial fracture toughness, are similar to those obtained by other techniques.

Because there are always differences between the elastic properties of the fibre and matrix, radial compressive stresses at the interface will usually accompany debonding. Consequently, when an embedded fibre fracture are debonding occurs, there will be a retraction of the fibre in the matrix, and a dissipation of elastic energy due to the frictional resistance. The effect of friction on G_{int} has not been satisfactorily described in previous work. The objective of this paper is to account for the effect of friction on the calculation of the toughness of interfacial debonding in single-fibre composites (SFC) from measurements of the debonding length accompanying the first fibre fracture. The approach presented is a logical continuation of the method previously published [16].

2. Theory

2.1. Approach

Let us consider an SFC under tensile loading parallel to the fibre axis. Assume an interfacial debonding of length, l_d, occurs after the first fibre break (Fig. 1). In a general case, for a specific interface and known elastic properties of the fibre and matrix, the strain energy release rate of the interface, G, can be represented as a function of the debond length, l_d, a parameter of loading, and a characteristic of friction.

$$G = G(l_d, \varepsilon, \mu) \tag{1}$$

where the parameter of loading $\varepsilon = \Delta/l$ is the average tensile strain (Fig. 2) and μ is the coefficient of friction of the interface. The function $G(l_d, \varepsilon, \mu)$ will be computed using a finite element analysis, and the debond length, $l_d = l_{d,\,arrest}$, upon its arrest at a constant strain,

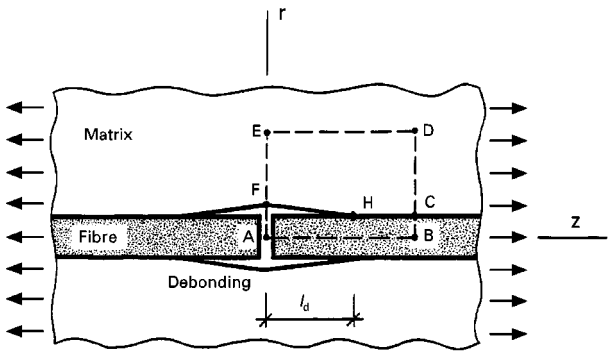

Figure 1 The general scheme of interfacial debonding.

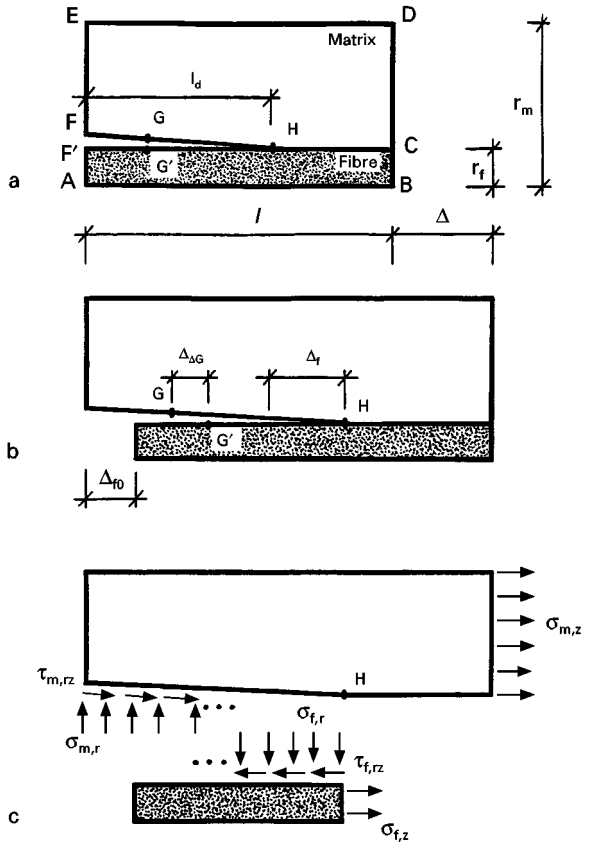

Figure 2 (a) Representative volume of SFC, (b) schematic illustration of its deformation, and (c) the stress state.

$\varepsilon = \varepsilon_{\text{arrest}}$, will be evaluated experimentally [16]. The strain $\varepsilon_{\text{arrest}}$ is approximately the *in situ* breaking strain of the embedded fibre. Thus, the fracture toughness of the interface, G_{int}, can be calculated as a function of μ

$$G_{\text{int}} = G(l_{\text{d, arrest}}, \varepsilon_{\text{arrest}}, \mu) \tag{2}$$

For calculation of $G(l_d, \varepsilon, \mu)$, we assume that, in a deterministic framework, there is a symmetry regarding the interfacial debonding in both r and z directions (z is the axis of symmetry). Hence, the energy release rate of the interface is defined as

$$G(l_d, \varepsilon, \mu) = -\frac{\delta U}{\delta A} = -\frac{\delta U}{2\pi r_f \delta l_d} \tag{3}$$

where U is the total energy of the one half of the SFC test specimen, $A = 2\pi r_f l_d$ is the debonded surface at one fibre end, and r_f is the fibre radius.

Deformation of the SFC considering the friction may be illustrated in Fig. 2. Here (Fig. 2a), F–H (F′–H) is the debonding zone, A–B is the axis of symmetry of the representative area of the SFC, and displacement Δ is considered as a parameter of loading (Fig. 2b). Mutual displacements of the fibre and matrix in the debonding zone $\Delta_{\Delta G} = \Delta_{G'} - \Delta_G$ are shown in Fig. 2b for the points G (matrix) and G' (fibre) on the interface ($r = r_f$). These displacements depend on the frictional properties. For example, if there is no friction at all ($\mu = 0$), then displacement $\Delta_{f0} \approx \Delta_f$ (Fig. 2b) because frictional shear stresses $\tau_{f,rz}$ and $\tau_{m,rz}$ (Fig. 2c) should be equal to zero (where f and m indicate fibre and matrix, respectively). In the limiting case of very high friction ($\mu \to \infty$), the displacements $\Delta_G \approx \Delta'_G$; $\Delta_{\Delta G} \approx 0$ and $\Delta_{f0} \to 0$. Therefore, two groups of external stresses acting on the system may be noted, namely the normal stresses $\sigma_{f,z}$ and $\sigma_{m,z}$ along the surfaces B–C and C–D, respectively, and frictional shear stresses $\tau_{f,rz}$ (surface F′–H) and $\tau_{m,rz}$ (F–H). The effect of normal and shear stresses along the surface D–E may be ignored at large values of the ratio r_m/r_f when the work of normal stresses along surfaces F(F′)–H is equal to zero, because there are no mutual displacements in the radial direction.

In the absence of thermal effects, plastic response, and damage accumulation, variation of the total energy δU may be written as

$$\delta U = \delta U_1 - \delta U_2 \tag{4}$$

where U_1 is the stored elastic energy and U_2 is the work of external stresses. Because loading is not a reversible process, work of the frictional stresses can be evaluated as the work of ordinary external stresses. Thus, taking into account that a contact problem should be generally considered in a non-linear statement, we have [26]

$$\begin{aligned}\delta U_1 = \delta\Bigg[& \int_{(A_{C-D})} \left(\int_0^{\Delta} \sigma_{m,z}\, d\Delta \right) dA \\ & + \int_{(A_{B-C})} \left(\int_0^{\Delta} \sigma_{f,z}\, d\Delta \right) dA \\ & - \int_{(A_{F'-H})} \left(\int_0^{\Delta_{G'}} \tau_{f,rz}\, d\Delta_{G'} \right) dA \\ & + \int_{(A_{F-H})} \left(\int_0^{\Delta_G} \tau_{m,rz}\, d\Delta_G \right) dA \Bigg]\end{aligned} \tag{5}$$

$$\begin{aligned}\delta U_2 = & \int_{(A_{C-D})} (\sigma_{m,z}\, \delta\Delta)\, dA + \int_{(A_{B-C})} (\sigma_{f,z}\, \delta\Delta)\, dA \\ & - \int_{(A_{F'-H})} (\tau_{f,rz}\, \delta\Delta_{G'})\, dA \\ & + \int_{(A_{F-H})} (\tau_{f,rz}\, \delta\Delta_G)\, dA\end{aligned} \tag{6}$$

were integration over A designates the integration over the surfaces defined in Fig. 2; $\sigma_{m,z}$, $\sigma_{f,z}$ are calculated at $z = l$; and $\tau_{f,rz}$, $\tau_{m,rz}$ are calculated at $r = r_f$. For the specific case of the stresses being linear

functions of displacements, one can rewrite Equation (4) as

$$\delta U = \frac{1}{2}\int_{(A_{C-D})} (\Delta\delta\sigma_{m,z} - \sigma_{m,z}\,\delta\Delta)\,dA + \frac{1}{2}\int_{(A_{B-C})} (\Delta\delta\sigma_{f,z} - \sigma_{f,z}\,\delta\Delta)\,dA - \frac{1}{2}\int_{(A_{F'-H})} (\Delta_{G'}\,\delta\tau_{f,rz} - \tau_{f,rz}\,\delta\Delta_{G'})\,dA + \frac{1}{2}\int_{(A_{F-H})} (\Delta_G\delta\tau_{f,rz} - \tau_{f,\,rz}\,\delta\Delta_G)\,dA \quad (7)$$

Let us consider the case when Δ is held constant and only l_d increases by δl_d (i.e. debonding at constant strain). Because there is no external work performed by stresses $\sigma_{m,z}$ and $\sigma_{f,z}$, the variation of the total energy can be calculated as

$$\delta U = \frac{1}{2}\int_{(A_{C-D})} (\Delta\delta\sigma_{m,z})\,dA + \frac{1}{2}\int_{(A_{B-C})} (\Delta\delta\sigma_{f,z})\,dA - \frac{1}{2}\int_{(A_{F'-H})} (\Delta_{G'}\delta\tau_{f,rz} - \tau_{f,rz}\delta\Delta_{G'})\,dA + \frac{1}{2}\int_{(A_{F-H})} (\Delta_G\delta\tau_{f,rz} - \tau_{f,rz}\delta\Delta_G)\,dA \quad (8)$$

At equilibrium, $\tau_{f,rz} = \tau_{m,rz}$ and, thus, the axis-symmetrical solution of Equation 3 may be written as

$$G(l_d, \varepsilon, \mu) = -\frac{\Delta}{2r_f}\int_{r_f}^{r_m}\left[\frac{\delta\sigma_{m,z}(r)}{\delta l_d}\right] r\,dr - \frac{\Delta}{2r_f}\int_0^{r_f}\left[\frac{\delta\sigma_{f,z}(r)}{\delta l_d}\right] r\,dr + \frac{1}{2}\int_0^{l_d}\left[\Delta_{\Delta G}(z)\frac{\delta\tau_{m,rz}(z)}{\delta l_d} - \tau_{m,rz}(z)\frac{\delta\Delta_{\Delta G}(z)}{\delta l_d}\right] dz \quad (9)$$

where $\Delta_{\Delta G} = \Delta_{G'} - \Delta_G$.

When the stresses are linear functions of ε, all components of energy are directly proportional to ε^2, and, therefore, the toughness may be finally calculated as

$$G_{int} = G(l_d = l_{d,arrest}, \varepsilon = \bar{\varepsilon}, \mu)\left(\frac{\varepsilon_{arrest}}{\bar{\varepsilon}}\right)^2 \quad (10)$$

where $\bar{\varepsilon}$ is the unit strain, chosen as $\bar{\varepsilon} = 1\%$ in the present paper.

2.2. Method of numerical realization

The following numerical procedure is used to evaluate $G(l_d, \varepsilon, \mu)$ with Equation 9. For a specific debonding length l_d, G will be evaluated at two different lengths, $l'_d = l_d - \Delta_{ld}/2$ and $l''_d = l_d + \Delta_{ld}/2$; all other parameters of the SFC test, including the average strain, ε, and coefficient of friction, μ, are held constant. Here, Δ_{ld} is a small length decrement chosen using a sequence of numerical analyses with different values of Δ_{ld} that define a required level of accuracy. If $\sigma'_{m,z}$, $\sigma'_{f,z}$, $\tau'_{m,rz}$, $\Delta'_{\Delta G}$ are the characteristics of the stress-strain state at $l_d = l'_d$, while $\sigma''_{m,z}$, $\sigma''_{f,z}$, $\tau''_{m,rz}$, $\Delta''_{\Delta G}$ are those at $l_d = l''_d$, we have for $\Delta_{ld} \to 0$.

$$\frac{\delta\sigma_{m(f),z}}{\delta l_d} \approx \frac{\sigma''_{m(f),z} - \sigma'_{m(f),z}}{\Delta_{ld}} \quad (11a)$$

$$\frac{\delta\tau_{m,rz}}{\delta l_d} \approx \frac{\tau''_{m,rz} - \tau'_{m,rz}}{\Delta_{ld}} \quad (11b)$$

$$\frac{\delta\Delta_{\Delta G}}{\delta l_d} \approx \frac{\Delta''_{\Delta G} - \Delta'_{\Delta G}}{\Delta_{ld}} \quad (11c)$$

$$\tau_{m,rz} \approx \frac{\tau'_{m,rz} + \tau''_{m,rz}}{2} \quad (11d)$$

$$\Delta_{\Delta G} \approx \frac{\Delta'_{\Delta G} + \Delta''_{\Delta G}}{2} \quad (11e)$$

and a numerical evaluation of $G(l_d, \varepsilon, \mu)$ may be written as

$$G(l_d, \varepsilon, \mu) \approx -\frac{\Delta}{2r_f\Delta_{ld}}\int_{r_f}^{r_m}(\sigma''_{m,z} - \sigma'_{m,z})\,r\,dr - \frac{\Delta}{2r_f\Delta_{ld}}\int_0^{r_f}(\sigma''_{f,z} - \sigma'_{f,z})\,r\,dr + \frac{1}{2\Delta_{ld}}\int_0^{l_d}(\Delta'_{\Delta G}\tau''_{m,rz} - \Delta''_{\Delta G}\tau'_{m,rz})\,dz \quad (12)$$

Numerical realization of Equation 12 may be simplified as well, because the function $\tau_{m,rz}(z)$ varies only slightly with z and may be considered as approximately constant. Therefore, $G(l_d, \varepsilon, \mu)$ may be evaluated as

$$\begin{aligned} G(l_d, \varepsilon, \mu) \approx & -\frac{\Delta}{2r_f\Delta_{ld}}\int_{r_f}^{r_m}(\sigma''_{m,z})r\,dr - \frac{\Delta}{2r_f\Delta_{ld}}\int_0^{r_f}(\sigma''_{f,z})\,r\,dr + \frac{\Delta}{2r_f\Delta_{ld}}\int_{r_f}^{r_m}(\sigma'_{m,z})\,r\,dr + \frac{\Delta}{2r_f\Delta_{ld}}\int_0^{r_f}(\sigma'_{f,z})\,r\,dr \\ & + \frac{1}{2\Delta_{ld}}\bar{\tau}''_{m,rz}\int_0^{l_d}(\Delta'_{\Delta G})\,dz - \frac{1}{2\Delta_{ld}}\bar{\tau}'_{m,rz}\int_0^{l_d}(\Delta''_{\Delta G})\,dz \\ = & \frac{1}{2\pi r_f\Delta_{ld}}(-W''_\sigma + W'_\sigma + \bar{\tau}''_{m,rz}g' - \bar{\tau}'_{m,rz}g'') \end{aligned} \quad (13)$$

where the following functions of the stress–strain state

$$W_\sigma = \pi\Delta\int_{r_f}^{r_m}[\sigma_{m,z}]\,r\,dr + \pi\Delta\int_0^{r_f}[\sigma_{f,z}]\,r\,dr \quad (14a)$$

$$\bar{\tau}_{m,rz} = \frac{1}{l_d}\int_0^{l_d}\tau_{m,rz}(z)\,dz \quad (14b)$$

$$g = \pi r_f\int_0^{l_d}[\Delta_{\Delta G}]\,dz \quad (14c)$$

may be calculated separately for each debonding length (l'_d, l''_d) using conventional methods of numerical integration.

2.3. Finite-element analysis

Numerical evaluation of the stress–strain state was carried out using a finite-element analysis (FE-code MARC [27]). The analysis was developed in a contact non-linear statement using an iterative procedure of approximation. The number of iterations used provided an accuracy of a least three digits for displacements. A typical FE-mesh is shown in Fig. 3, illustrating a simulation of a SFC deformation at $\varepsilon = 5\%$ ($l_d = 20\,\mu m$; $r_f = 5\,\mu m$). The following boundary conditions are defined for an axially symmetric model:

(a) $\Delta_r = 0$ along the axis A–B;
(b) $\Delta_z = 0$ along the axis E–F;
(c) $\Delta_z = \Delta$ along the axis B–D;
(d) a continuity condition for displacements is fulfilled along the surface H − C;
(e) a contact condition for two elastic bodies is fulfilled along surfaces F − H (matrix) and F′ − H (fibre): mutual displacements in th contact zone $\Delta_{\Delta G} = \Delta_{G'} - \Delta_G$ can be seen in Fig. 3.

Because non-zero components of the stress-state exist in any point of the system, the boundary conditions, strictly speaking, represent a finite volume model of a SFC. However, variations (increments) of stresses $\sigma_{m,z}$ and $\sigma_{f,z}$ with increasing debonding length should be close to zero in distant areas. Thus, we have chosen A–B = $50\,\mu m \approx 10r_f$ and B–D = $30\,\mu m \approx 6r_f$ to be sufficiently large to provide satisfactory approximation of the results for infinite volume.

2.4. Model of friction

Although the friction phenomenon can be taken into account using different FE computer codes, including MARC [27], the practical realization has some difficulties. While, for a very fine mesh and relatively uniform stress distribution, the result is most acceptable, the convergence process is often too slow when there is a significant variability of the stress state. Thus, a simple friction model, using a relatively coarse FE-mesh, is introduced.

The friction model uses an equilibrium condition written in terms of stresses. Because the displacement Δ_{f0} (Fig. 2b) reduces with increasing coefficient of friction μ, a unique monotonic function $\Delta_{f0} = \Phi(\mu)$ may be determined in principle. Conversely, an inverse function $\mu = \Phi^{-1}(\Delta_{f0})$ may be calculated as well (here, Φ^{-1} is an inverse function, not an inverse value!). In other words, displacement Δ_{f0} may be used as an input (i.e. a parameter of the friction) instead of the coefficient of friction. Therefore, $\Delta_z = \Delta_{f0}$ should be introduced as an additional boundary condition for the point F′. For a relatively long debonding length, this condition may be written for the whole surface A–F′.

A value for μ may therefore be calculated using the results of the FE-analysis and the appropriate equilibrium equations. Let us consider a part of the fibre between points F′ and H (Fig. 2c). The balance of forces in the z-direction may be written as

$$2\pi r_f \int_0^{l_d} \tau_{f,rz}(z, r = r_f)\,dz = \int_0^{r_f} \sigma_{f,z}(z = l_d, r)\,2\pi r\,dr \tag{15}$$

We assume that the frictional response may be determined by a Coulomb law

$$\tau_{f,rz}(z, r = r_f) = -\mu\sigma_{m,r}(z, r = r_f) \tag{16}$$

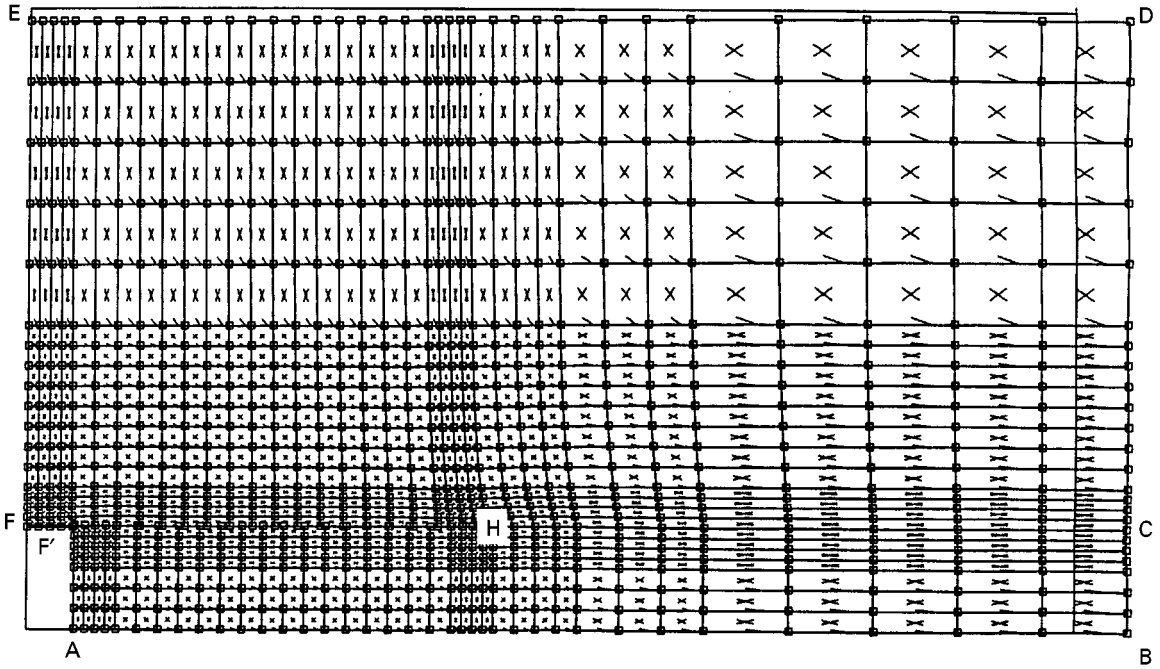

Figure 3 Typical FE-mesh reflecting deformation of S-glass/Soft epoxy SFC at $\varepsilon = 5\%$.

where $\sigma_{m,r}(z, r = r_f)$ are compressive stresses in the radial direction at the peripheral surface of the fibre. Thus, taking into account an axially symmetric statement of the problem we obtain

$$\mu = -\frac{\int_0^{r_f} \sigma_{f,z}(z = l_d, r)\, r\,dr}{r_f \int_0^{l_d} \sigma_{m,r}(z, r = r_f)\, dz} \quad (17)$$

While there is no friction when $\sigma_{m,r}(z, r = r_f) \geq 0$, this limitation can be easily taken into account using an appropriate numerical procedure of integration of Equation 17. An algorithm for application of the model consists of two steps. First, the analysis is developed for a set of magnitudes $\Delta_{f0}^{(i)}$, $i = 1, \ldots, n$ where n is the number of independently solved problems. Values of $\mu^{(i)}$ and characteristics of the stress–strain state are calculated for each characteristic $\Delta_{f0}^{(i)}$. Second, the functions $W_\sigma(\mu)$, $\bar{\tau}_{m,rz}(\mu)$, $g(\mu)$ are determined using interpolation of all points. The function $G(\mu)$, defined by Equation 13, may then be evaluated.

3. Numerical results

3.1. Materials

Embedded single-fibre composite specimens were made for measuring the effect of surface treatments on the interfacial fracture toughness of glass fibre/epoxy composites [16]. The following analysis is a continuation of this work in which the effect of friction on the calculated values of G is illustrated. The matrices, fibres, and compositions of the specimens are reproduced below [16].

Stiff epoxy: diglycidyl ether of bisphenol-A (DER 331, Dow Chemical) cured with 14 p.h.r. by weight of tetra-ethylene-pentamine (DEH 26, Dow Chemical).

Soft epoxy: a mixture of 70/30 by weight of DER 331 and diglycidyl-ether of propylene-glycol (DER 732, Dow Chemical) cured with 11.5 p.h.r. by weight of DEH 26.

S-glass fibres (Owens Corning), with an average diameter of 10 μm: these fibres were supplied with two different surface treatments, the first being a starch coating and the second a commercial epoxy-compatible sizing. The starch-coated fibres were either used as-received or UV–ozone cleaned for 1 h. The cleaned (bare) fibres were then surface treated in two different ways. Some of the fibres were coated with an epoxy resin mixture 50/50 by weight of DER 331 and DER 732 cured with 10 p.h.r. by weight of DEH 26 from a solution of 0.3 wt vol % of epoxy resin in acetone. The bottom of a glass petri dish was filled with the coating solution and the fibres were added for a period of 5 min. The fibres were then removed from the solution and allowed to dry in air for a period of 10 min, after which they were placed into a vaccum oven and dried at room temperature under vacuum for 30 min. The oven was brought up to atmospheric pressure, and the epoxy resin coating was cured at 80 °C for 2h. The remaining UV–ozone cleaned fibres were coated with methyl-trimethoxy-silane (United Chemical Technology). The silane was applied by immersing the fibres for 5 min in a primer solution of 5% silane and 5% water in 90% methanol by volume. After removal from the primer solution, the fibres were dried in air for 10 min and then placed in a oven at 100 °C for 30 min.

Water-sized E-glass fibres (Union Carbide), with an average diameter of 13 μm: these fibres were UV–ozone cleaned for 0.5 h in order to remove organic impurities. some of the UV–ozone cleaned E-glass fibres were coated with methyl-trimethoxy-silane following the same procedure described above for the S-glass fibres. The elastic properties of the components are shown in Table I.

3.2. Effect of non-linearity

While a general solution of Equation 6 is non-linear, we will show that for values of $\varepsilon < 10\%$, the non-linearity can be neglected and Equations 9 and 10 can be used to evaluate the interfacial toughness in the SFC. Let us consider, for example, results of FE "contact" analysis for the S-glass/soft epoxy SFC with a debonding length $l_d = 20$ μm. Fig. 4 illustrates the nearly linear dependence on ε of the displacements in points A (in the z-direction) and D (in the r-direction), as well as stresses at points B and D in the z-direction. The same regularities have been noted for the other SFCs at different l_d. Because the strains at the first break in the present study are all less than 6–7% [16], we are able to calculate the toughness using the simple linear statement.

3.3. Stress–strain state

A typical distribution of $\sigma_{m,r}(z, r = r_f)$ at different values of Δ_{f0} for the S-glass/soft epoxy SFC with a debond length $l_d = 20$ μm and $\varepsilon = 1\%$ are shown in Fig. 5. The FE solutions in the contact zone close to the debonding tip and the fibre break are too rough even for a relatively fine mesh. Thus, the following approximations regarding stresses $\sigma_{m,r}(z, r = r_f)$ are introduced, as shown in Fig. 6.

(a) the stresses in the vicinity of the fibre break are considered as constant, i.e.

$$\sigma_{m,r}(z \leqslant z_0, r = r_f) = \sigma_{m,r}(z = z_0, r = r_f);$$

(b) the stresses in the vicinity of the crack tip are ignored ($\sigma_{m,r}(z \geqslant z_k, r = r_f) = 0$), because $\sigma_{m,r}(z \geqslant z_k, r = r_f) \geqslant 0$ and no frictional shear stresses are in this zone.

The stresses $\sigma_{m,r}$ shown in Fig. 6 are calculated at $\mu = 2.21$ ($\Delta_{f0} = 0.40$), using the FE code and the

TABLE I Properties of the components

Component	Modulus of elasticity (GPa)	Poisson's ratio
Stiff epoxy	2.9	0.35
Soft epoxy	1.6	0.35
S-glass fibre	86.9	0.22
E-glass fibre	72.0	0.22

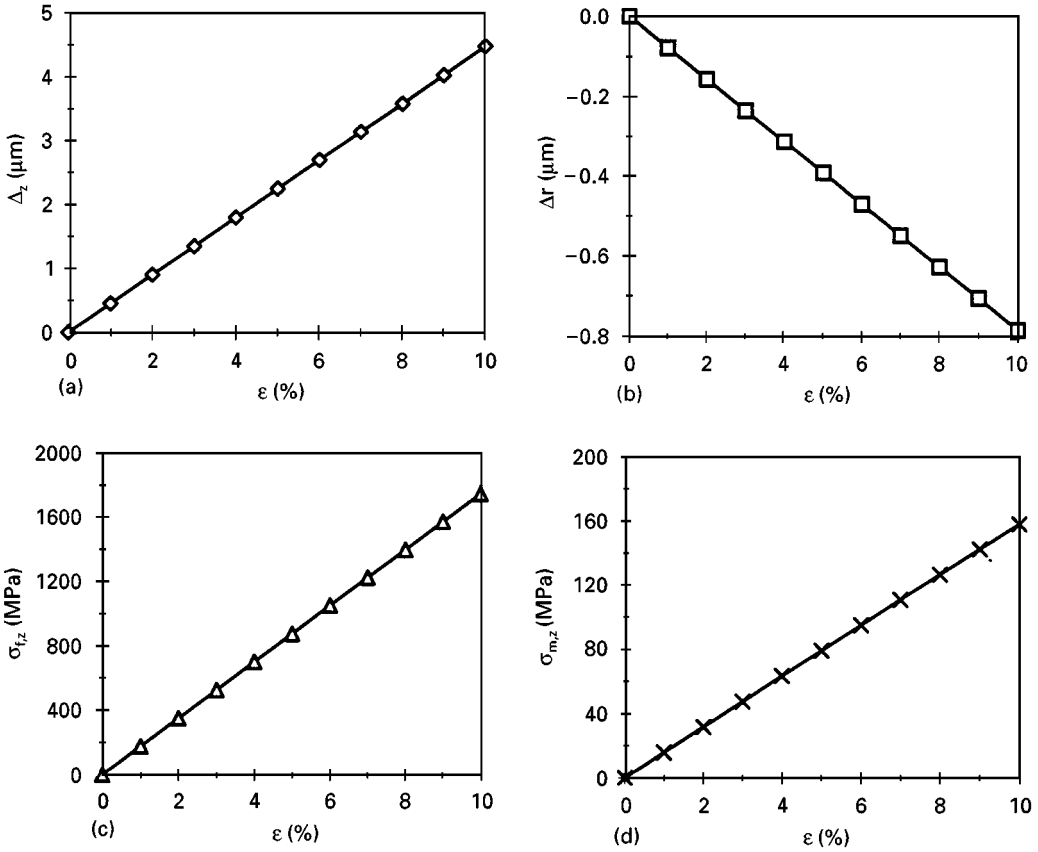

Figure 4 Dependencies of displacements (a) A, (b) D, stresses (c) B, and (d) D on ε.

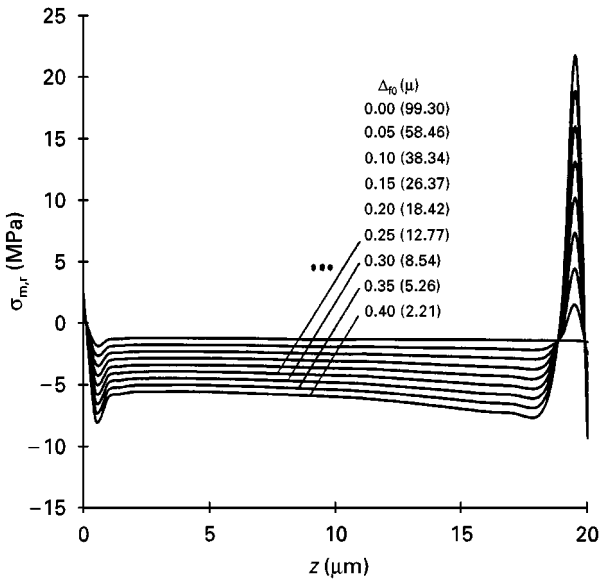

Figure 5 Distributions of $\sigma_{m,\,r}$ $(z, r = r_f)$. $\Delta_{f0}(\mu)$: (1) 0.00 (99.30); (2) 0.05 (58.46); (3) 0.10 (38.34); (4) 0.15 (20.37), (5) 0.20 (18.42); (6) 0.25 (12.77); (7) 0.30 (8.54), (8) 0.35 (5.26); (9) 0.40 (2.21).

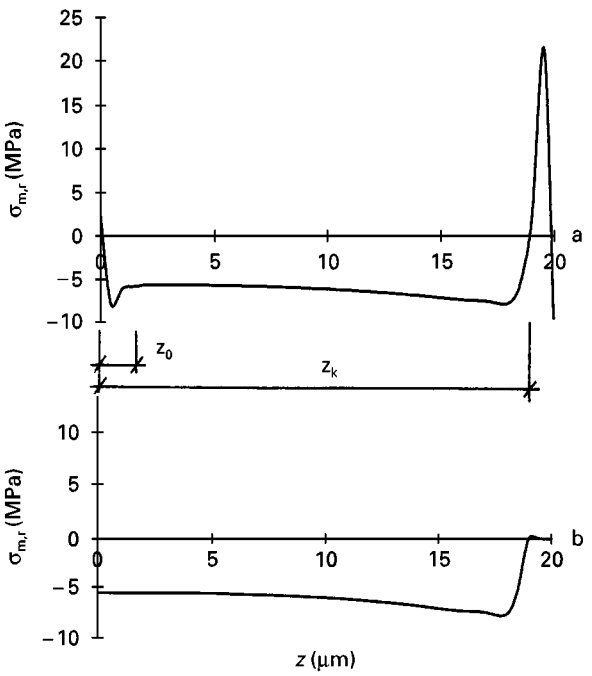

Figure 6 Distributions of $\sigma_{m,\,r}$ $(z, r = r_f)$ at $\mu = 2.21$ calculated by (a) FEA and (b) its modelling.

approximations described above. Although from the principles of equilibrium, the functions $\sigma_{m,r}(z, r = r_f)$ and $\sigma_{f,r}(z, r = r_f)$ should be equal, FE contact analysis will always produce a certain difference between these stresses. In all future analyses, we use $\sigma_{m,r}$, because these stresses reflect the more detailed mesh for the matrix (Fig. 3), and, therefore, may be considered as more accurate than the estimates of $\sigma_{f,r}$. The displacements Δ_G, Δ'_G, and $\Delta_{\Delta G}$ are shown in Fig. 7 for $\mu = 2.21$ ($\Delta_{f0} = 0.40$).

The influence of friction on the incremental change of energy can be analysed by considering separately the effects of the normal stresses $\sigma_{f,z}$ $(\sigma_{m,z})$ and shear stresses $\tau_{m,rz}$ Fig. 8 shows the calculated work of these external stresses, W_σ and W_τ respectively, for the S-glass/soft epoxy SFC at $l_d = 20$ μm; $\varepsilon = 1\%$. One can see that W_σ (work of $\sigma_{f,z}$)$\sigma_{m,z}$) at $z = l$) is

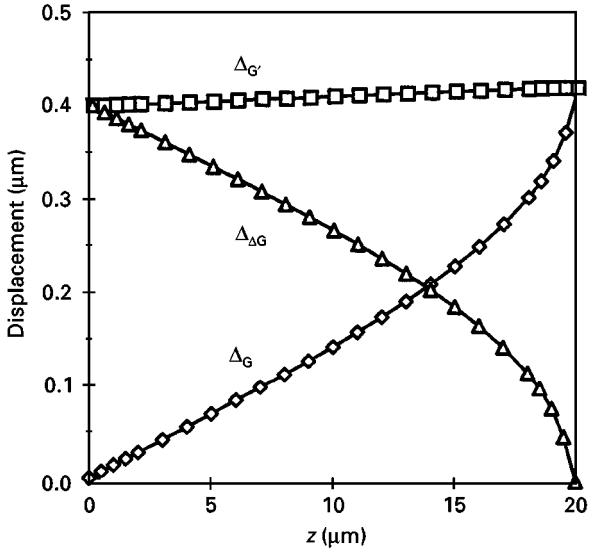

Figure 7 Distributions of $\Delta_G(z)$, and $\Delta'_G(z)$.

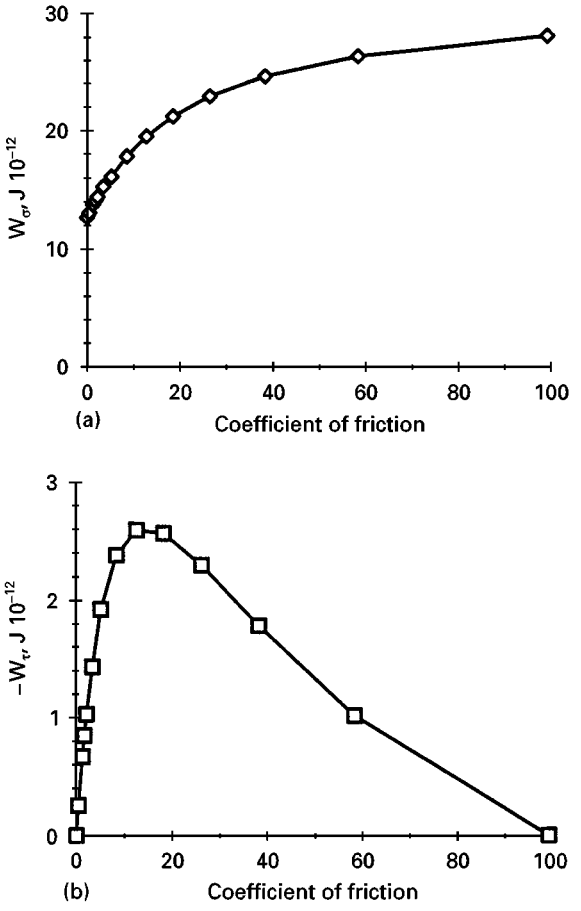

Figure 8 Dependencies of (a) W_σ and (b) $-W_\tau$ on μ.

a monotonically increasing function of μ (Fig. 8a). The increase is a result of the fact that an increase of μ results in higher stiffness of the system. Thus, W_σ approaches a maximum as $\mu \to \infty$. The work of frictional shear stresses $\tau_{m,rz}$ at $r = r_f$, W_τ, however, must show a maximum at an intermediate value of μ. While the stress $\tau_{m,rz}$ monotonically increases with μ, mutual displacements $\Delta_{\Delta G}$ decrease. In the limit of $\mu = 0$, $\tau_{m,rz} = 0$, $\Delta_{\Delta G} \to \max$ and, therefore, $W_\tau = 0$. When $\mu \to \infty$, $\Delta_{\Delta G} = 0$, $\tau_{m,rz} \to \infty$, and, therefore, $W_\tau = 0$, as shown in Fig. 8b. The magnitudes of W_σ are approximately one order higher than W_τ, and the difference is determined by the volume of the SFC. The effect of W_τ cannot be neglected, however, because the toughness of the interface depends on the incremental change of the energy, δU, rather than its absolute value.

3.4. Example of the analytical procedure

Let us consider the calculation of $G(l_d, \varepsilon, \mu)$ at $l_d = 19.5$ μm; $\varepsilon = 1\%$ for the S-glass/soft epoxy SFC. The debonding lengths $l_d' = 19$; $l_d'' = 20$ μm (i.e. $\Delta_{ld} = 1$ μm) are introduced for numerical realization of Equation 13. The values of W_σ, $\tau_{m,rz}/\mu$, and g as functions of μ are shown in Fig. 9, where the values of μ have been calculated using Equation 17 for different magnitudes of Δ_{f0}. The respective functions of μ may be approximated by the following second-order polynomials

$$W'_\sigma = 12.822 + 0.8432\mu - 0.0302\mu^2 \quad (18a)$$

$$W''_\sigma = 12.698 + 0.8654\mu - 0.0336\mu^2 \ (10^{-12}\text{J}) \quad (18b)$$

$$\bar{\tau}'_{m,rz}/\mu = 6.9977 - 0.3456\mu + 0.0613\mu^2 \ (\text{MPa}) \quad (18c)$$

$$\bar{\tau}''_{m,rz}/\mu = 6.6923 - 0.3222\mu + 0.0145\mu^2 \ (\text{MPa}) \quad (18d)$$

$$g' = [85.84 + 5.378\mu - 0.2313\,\mu^2](l_d/l'_d)^2 \ (\mu\text{m}^2) \quad (18e)$$

$$g'' = [90.89 + 5.662\mu - 0.1986\mu^2](l_d/l''_d)^2 \ (\mu\text{m}^2) \quad (18f)$$

The ratios $(l_d/l'_d)^2$ and $(l_d/l''_d)^2$ appear in the approximation of g' and g'', respectively, since the function $\Delta_{\Delta G}(z)$ has a roughly triangular form. The integrals, defined by Equation 14, therefore, are reasonably approximated using the square of the above-mentioned ratios. The energy release rate for debonding at the interface, $G(l_d, \varepsilon, \mu)$, can then be approximated using Equation 13 in the following form

$$G(l_d, \varepsilon, \mu) = G_\sigma(l_d, \varepsilon, \mu) + G_\tau(l_d, \varepsilon, \mu) \quad (19)$$

where

$$G_\sigma = -\frac{1}{2\pi r_f \Delta_{ld}}(W''_\sigma - W'_\sigma) \quad (20)$$

$$G_\tau = -\frac{1}{2\pi r_f \Delta_{ld}}(\bar{\tau}'_{m,rz} g'' - \bar{\tau}''_{m,rz} g') \quad (21)$$

Equations 19–21 are plotted as functions of the coefficient of friction, μ, in Fig. 10. In the limit $\mu \to \infty$, there is absolute continuity in the debonding area F(F′)H and, therefore, no effect of l_d at all. In other words, $G_\sigma(\mu \to \infty) \to 0$, $G_\tau(\mu \to \infty) \to 0$, and thus, $G(\mu \to \infty) \to 0$. At practical values of μ, however, the effect of friction on the calculated values of the interfacial toughness cannot be neglected.

3.5. Effect of debonding length and interface treatment

The dependence of $G(l_d, \mu)$ for the *S*-glass/soft epoxy SFC is presented in Fig. 11a at $\varepsilon = 1\%$. For a constant strain, ε, the calculated value of $G(l_d)$ decreases with increasing coefficient of friction at all values of debond

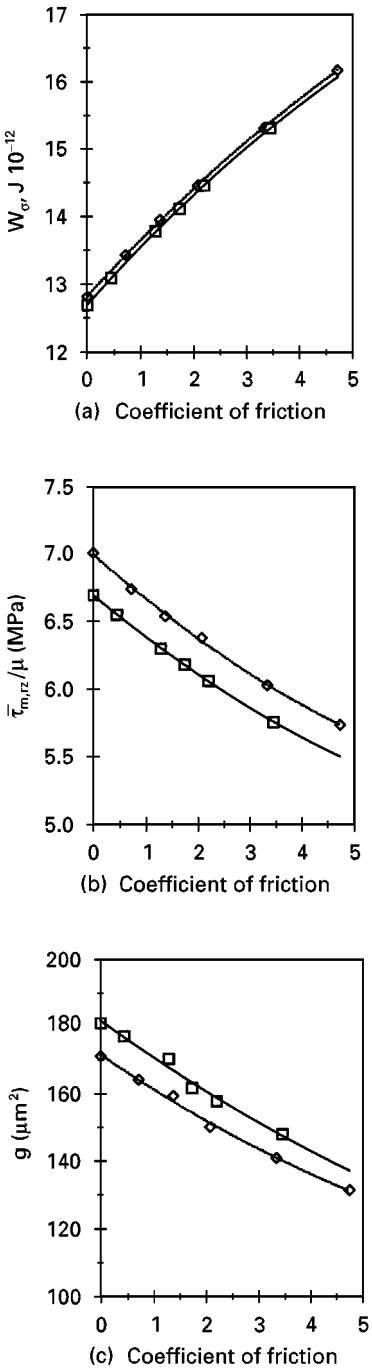

Figure 9 Dependencies of (a) W_σ, (b) $\bar{\tau}_{m,\,rz}/\mu$, and (c) g on debonding lengths (◇) l'_d and (□) l''_d.

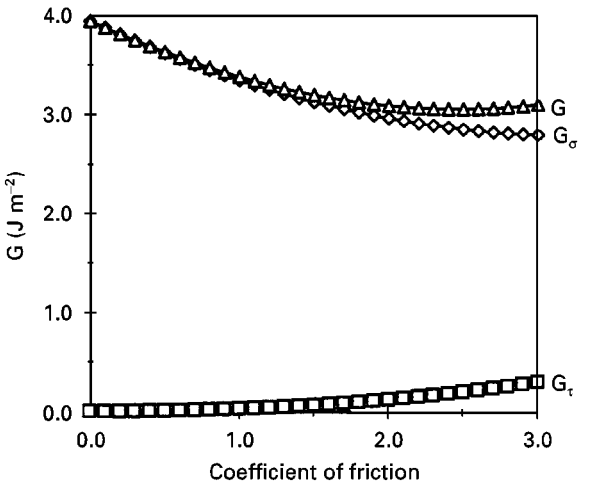

Figure 10 Dependencies of G_σ, G_τ, and G on μ.

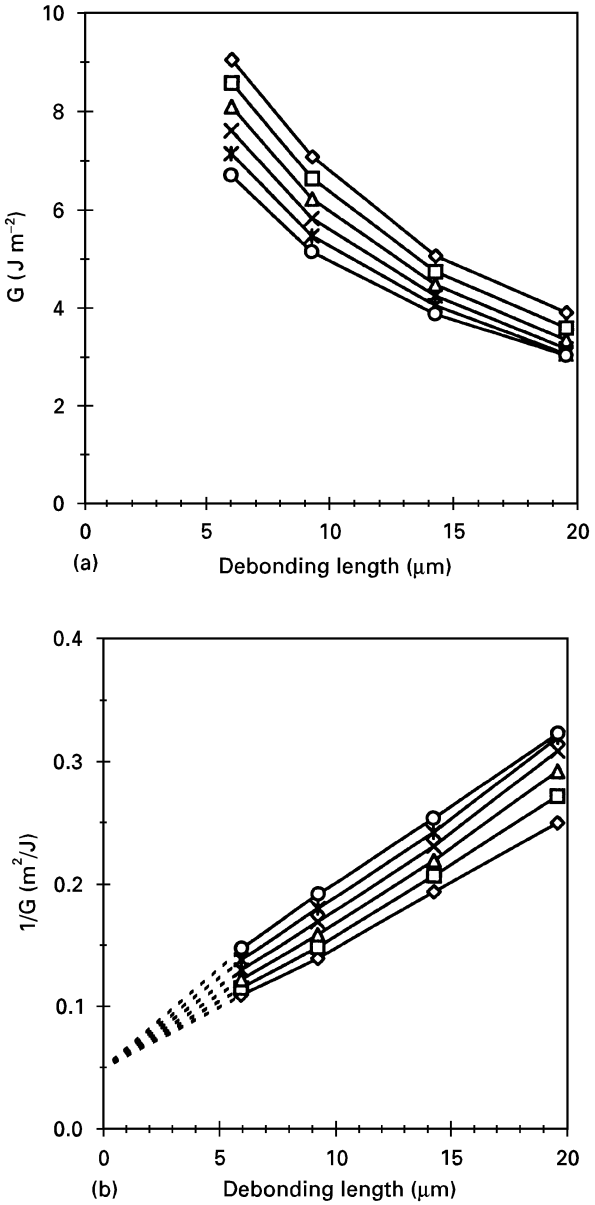

Figure 11 Dependencies of (a) G and (b) $1/G$ on μ and l_d. μ: (◇) 0.0, (□) 0.5, (△) 1.0, (×) 1.5, (∗) 2.0, (○) 2.5.

length. The inverse of the fracture toughness at $\mu = 0$ is nearly a linear function of the debonding length (Fig. 11b). Extrapolation to $l_d = 0$ gives $1/G = 0.0485\ m^2\ J^{-1}$ ($G = 20.618\ J\ m^{-2}$) [23]. Because at $l_d \to 0$ the effect of friction becomes negligible, one can expect that $1/G(l_d = 0, \mu \neq 0) \approx 1/G(l_d = 0, \mu = 0)$. Thus, the dotted lines drawn in Fig. 11b reflect the expected dependencies of $1/G(l_d, \mu)$ at short l_d. Although the approximation of $1/G(l_d)$ is close to linear at $\mu = 0$, the approximations at $\mu > 1.0$ are slightly non-linear.

Experimental data of the debonding length accompanying the first fibre fracture in the (S-glass, E-glass)/(soft and stiff epoxy) SFCs with three different fibre surface treatments have been reported previously [16]. Calculated values of G were based on a FE contact analysis with $\mu = 0$. Results of calculations using Equation 10 and considering the effect of friction, are shown in Table II and in Fig. 12 for

TABLE II Characteristics of debonding and fracture toughness

Type	Epoxy/glass	Fibre surface treatment	ε_{arrest} [16] (%)	$l_{d,arrest}$ [16] μm	$G_{int}(\mu = 0)$ (J m^{-2})	$G_{int}(\mu = 1)$ (J m^{-2})	$G_{int}(\mu = 3)$ (J m^{-2})
A	Stiff/S	Starch	5.2 ± 0.5	5.6 ± 0.3	327.1	295.8	206.7
B	Stiff/S	Soft epoxy coating	4.8 ± 0.4	5.5 ± 0.6	278.7	252.0	176.1
C	Stiff/S	Methyltrimethoxysilane	4.6 ± 0.3	9.4 ± 1.0	187.7	160.6	119.0
D	Soft/S	Starch	6.1 ± 0.7	9.2 ± 1.0	264.5	232.2	181.7
E	Soft/S	Soft epoxy coating	5.8 ± 0.6	9.3 ± 0.8	234.2	206.5	160.7
F	Soft/S	Methyltrimethoxysilane	5.1 ± 0.4	14.2 ± 2.3	132.5	117.2	97.0
G	Stiff/E	Methyltrimethoxysilane	2.5 ± 0.2	3.9 ± 0.6	72.5	62.6	48.1
H	Soft/E	Methyltrimethoxysilane	2.4 ± 0.2	5.8 ± 0.4	53.4	47.8	38.0

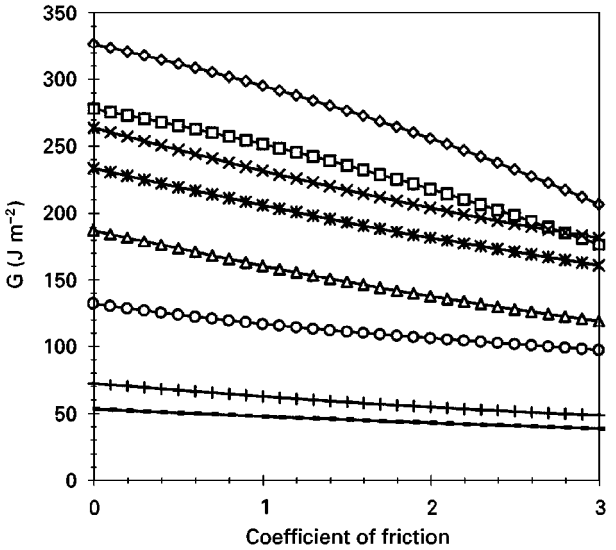

Figure 12 Dependencies of G_{int} on μ. Type: (◇) A, (□) B, (△) C, (×) D, (∗) E, (○) F, (+) G, (−) H.

$0 \leqslant \mu \leqslant 3$. Reduction in the calculated values of fracture toughness because of the friction is of the order of 10%–15% with $\mu = 1.0$ and 27%–37% with $\mu = 3.0$ (Table II). The SFCs containing E-glass fibres possess much lower toughness than similar composites using S-glass fibres. Moreover, there is significant difference in the values of G between, for example, the Type "C" and "G" systems in spite of the fact that both the fibre surface treatment (methyltrimethoxysilane) and the matrix (Stiff) are identical in the two composites. Numerically, the primary difference between the two systems is in the strain-at-first break of the fibres, i.e. $\varepsilon_{arrest} = 2.4\%–2.5\%$ for E-glass and 4.6%–6.1% for S-glass fibres, thus creating a four to five times higher level of stored elastic energy at the point of initiation of debonding in the latter system. It appears that a complete evaluation of this result must include an analysis of the elasto-plastic deformations of the matrix on the calculation of G_{int}. Work is in progress along these lines.

4. Conclusions

1. An analytical–experimental analysis of a SFC can account for friction between fibre and matrix in the debonding zone. The approach is based on an exact analytical solution, while characteristics of the stress–strain state are determined from a FE-analysis in a contact statement. The debonding length at the strain at first break is obtained from experiments on SFC.

2. Numerical analysis of a range of SFC systems shows that non-linearity of the contact statement may be neglected within a range of loading of practical interest. Thus, a simpler linear solution (Equations 9 and 10) may be used for the analysis.

3. The model chosen to analyse the effect of friction allows direct to calculation of the coefficient of friction. As a result, a relatively coarse FE-mesh may be used for calculating the frictional shear stresses in an efficient manner.

4. The calculated value of interfacial fracture toughness decreases when the effect of friction is included in the model. The magnitude of the decrease depends on the elastic properties of fibre and matrix, the debonding length, the strain at first fibre break, and fibre surface treatment.

5. Because there is virtually no experimental information on the coefficient of friction between fibres and matrix in a composite material, independent experimental characterization of the friction is a significant problem for future research.

Acknowledgement

The authors thank Dr M. L. Accorsi for valuable consultations and comments regarding application of the FE-code MARC [27].

References

1. A. T. DIBENEDETTO, *Compos. Sci. Technol.* **42** (1991) 103.
2. B. W. ROSEN, *AIAA J.* **2** (1964) 1985.
3. W. A. FRASER, F. H. ANCKER, A. T. DIBENEDETTO and B. ELBIRLI, *Polym. Compos.* **4** (1983) 238.
4. A. N. NETRAVALI, R. B. HENSTENBURG, S. L. PHOENIX and P. SCHWARTZ, *ibid.* **10** (1989) 226.
5. W. A. CURTIN, *J. Mater. Sci.* **26** (1991) 5239.
6. A. T. DIBENEDETTO and M. R. GURVICH, *Compos. Sci. Technol.*, in press.
7. R. B. HENSTENBURG and S. L. PHOENIX, *Polym. Compos.* **10** (1989) 389.
8. H. D. WAGNER and A. EITAN, *Appl. Phys. Lett.* **56** (1990) 1965.
9. R. GULINO and S. L. PHOENIX, *J. Mater. Sci.* **26** (1991) 3107.

10. A. DIANSELMO, M. L. ACCORSI, and A. T. DIBENEDETTO, *Compos. Sci. Technol.* **44** (1992) 215.
11. M. J. PITKETHLY, J. P. FAVRE, U. GAUR, F. FAKUBOWSKI, S. F. MUDRICH, D. L. CALDWELL, L. T. DRZAL, M. NARDIN, H. D. WAGNER, L. DILANDRO, A. HAMPE, F. P. ARMISTEAD, M. DESAEGER and I. VERPOEST, *ibid.* **48** (1993) 205.
12. H. D. WAGNER and S. LING, *Adv. Compos. Lett*. **2** (1993) 169.
13. H. D. WAGNER, J. A. NAIRN and M. DETASSIS, *Appl. Compos. Mater*. **2** (1995) 107.
14. A. T. DIBENEDETTO, S. M. CONNELLY, W. C. LEE and M. L. ACCORSI, *J. Adhesion* **52** (1995) 41.
15. R. J. SCHEER and J. A. NAIRN, *ibid*., **53** (1995) 45.
16. A. PEGORETTI, M. L. ACCORSI and A. T. DIBENEDETTO, *J. Mater. Sci*., **31** (1996) 6145.
17. S. MOSTOVOY and E. J. RIPLING, *J. Appl. Polym. Sci.* **10** (1966) 1351.
18. A. T. DIBENEDETTO and P. J. LEX, *Polym. Eng. Sci.* **29** (1989) 543.
19. E. L. M. ASLOUN, M. NARDIN and J. SCHULTZ, *J. Mater. Sci.* **24** (1989).
20. V. RAO and L. T. DRZAL, *Polym. Compos.* **12** (1991) 48.
21. A. HAMPE and C. MAROTZKE, in "Proceedings of the 3rd International Conference on Deformation and Fracture of Composites", Guildford, UK, March 1995, p. 132.
22. J. A. NAIRN and Y. C. LIU, *Int. J. Solid. Struct*., submitted.
23. A. T. DIBENEDETTO and M. R. GURVICH, *Compos. Sci. Technol*., submitted.
24. A. T. DIBENEDETTO, in "Proceedings of the 6th International Conference on Composite Interface", Zichron Yaacov, 5–8 May 1996.
25. A. T. DIBENEDETTO, A. PEGORETTI and M. R. GURVICH, in "Proceedings of the 5th World Congress of Chemical Engineering", San Diego, CA, 14–18 July 1996.
26. J. G. WILLIAMS, "Fracture Mechanics of Polymers" (Ellis Horwood, Chichester, 1984) ch. 2, pp. 21–31.
27. "MARC, Vol. A. User Information" (MARC Corp., Palo Alto, CA, 1994).

Received 15 January 1997
and accepted 15 May 1998